Low temperature processed MnCo2O4 and MnCo1.8Fe0.2O4 as effective protective coatings for solid oxide fuel cell interconnects at 750 °C

Molin, Sebastian; Jasinski, P.; Mikkelsen, Lars; Zhang, W.; Chen, Ming; Hendriksen, Peter Vang

Published in:
Journal of Power Sources

Link to article, DOI:
10.1016/j.jpowsour.2016.11.011

Publication date:
2016

Document Version
Peer reviewed version

Low temperature processed $MnCo_2O_4$ and $MnCo_{1.8}Fe_{0.2}O_4$ as effective protective coatings for Solid Oxide Fuel Cell interconnects at 750°C

S.Molin[1]*, P. Jasinski[2], L. Mikkelsen[1], W. Zhang[3], M. Chen[1], P.V. Hendriksen[1]

[1.] Department of Energy Conversion and Storage, Technical University of Denmark, Frederiksborgvej 399, 4000 Roskilde, Denmark

[2.] Faculty of Electronics, Telecommunications and Informatics, Gdansk University of Technology, Narutowicza 11/12, 80-233 Gdansk, Poland

[3.] School of Materials Science and Engineering, Jilin University, 2699 Qianjin Street, Changchun 130012, China

*corresponding author: Sebastian Molin, DTU Energy, Frederiksborgvej 399, 4000 Roskilde, Denmark, tel: +45 46 77 52 96, e-mail: sebmo@dtu.dk

Abstract

In this study two materials, $MnCo_2O_4$ and $MnCo_{1.8}Fe_{0.2}O_4$ are studied as potential protective coatings for Solid Oxide Fuel Cell interconnects working at 750°C. First powder fabrication by a modified Pechini method is decribed followed by a description of the coating procedure. The protective action of the coating applied on Crofer 22 APU is evaluated by following the area specific resistance (ASR) of the scale/coating for 5500 hours including several thermal cycles. The coating is prepared by brush painting and has a porous structure after deposition. Post mortem microstructural characterization performed on the coated samples shows good protection against chromium diffusion from the chromia scale ensured by a formation of a dense reaction layer. This study shows, that even without high temperature sintering and/or reactive sintering it is possible to fabricate protective coatings based on MnCo spinels.

Keywords:

protective coating; high temperature corrosion; solid oxide fuel cell; interconnect; spinel; electrical conductivity;

Introduction

High temperature ceramic solid oxide cells (including fuel cells and electrolysis cells) are gaining attention due to their potential to reach high electrical efficiencies. Working temperature in the range from 700°C to 800°C offers high electrochemical performance without use of expensive catalysts. Due to recent advances in electrode development, the operation temperature of the fuel cells can be reduced from 800°C to around 750°C without significant shortcomings with respect to performance [1,2]. One of the most important issues hindering their more widespread commercialization is long-term durability of the cells and stacks. One of the major degradation phenomena is caused by the steel interconnects in the stack. Due to the growth of a poorly conductive oxide the electrical resistance of the interconnect increases over time. This results in an increase of the ohmic resistance of the stack. Another important degradation process related to the interconnect is the evaporation/diffusion of chromium to the active oxygen electrodes, where it results in an increase of the polarization resistance [3]. Commonly used cathode materials react heavily with Cr species and efforts to find Cr-resistant cathodes have only been moderately successful [4,5]. These two phenomena can cause an irreversible and severe degradation of the fuel cell stack.

Stainless steel has become the preferred interconnect material for planar SOFC stacks in the recent years. Its advantages with respect to the previously used ceramic interconnects are lower cost and simplified processing [6–10]. Crofer 22 APU is the most commonly used alloy in SOFC applications

[11,12]. Specifically designed for use at high temperatures, it contains ~22 wt.% of chromium and ~0.5 wt.% of Mn and some other minor alloying elements. Small addition of Mn to the alloy causes formation of a MnCr spinel on top of the chromia scale during the oxidation. This limits chromium evaporation due to lowered chromium activity on the surface. However, tests have shown that in order to operate fuel cells effectively with sufficiently low degradation rates, an additional coating blocking chromium outward diffusion and evaporation is required [13].

Among many possible coatings [14–21], manganese cobalt spinels were studied extensively as protective coatings for SOFC/SOEC interconnects [14,22]. These materials are compatible with contact layer materials in the fuel cells and have also proven to effectively block chromium outward diffusion and evaporation. As shown by Wu et al. [13], application of Mn-Co spinel to an interconnect resulted in much lower degradation of a solid oxide fuel cell, compared to a setup with uncoated steel. Similar results were shown by Yang et al. [23]. Long-term oxidation behavior of a spinel coated 441 stainless steel was reported by Stevenson et al. [24]. In the present study a 9000 hours long electrical characterization was performed at 800°C. Samples were coated with either $Mn_{1.5}Co_{1.5}O_4$ or $Mn_{1.475}Co_{1.475}Ce_{0.05}O_4$. The coated samples had much smaller initial ASR value and also smaller degradation rate than the uncoated reference. Addition of Ce to the coating further improved oxide scale adhesion. Kidner et al. [25] tested $Mn_{1.5}Co_{1.5}O_4$ coatings on 441 and Crofer 22 APU. For comparison, samples with and without “reduction firing” (based on first the reduction of the coating and then the re-oxidation of the coating) were studied measuring cross-scale resistance. For both steels, the authors reported that samples without a reduction firing have much higher resistance and also that the ASR increased at a higher rate. After only 1000 hours test ASR values exceeded ~100 mΩ cm^2. The authors concluded that a reduction step is required to obtain a sufficiently dense, stable microstructure of the coating.

In comparison to pure Co_3O_4 spinel, addition of Mn raises the electrical conductivity by about one order of magnitude and improves matching of thermal expansion coefficient with that of the

stainless steel. Also in terms of the cost and toxicity, replacing Co with Mn is advantageous. From different compositions of $(Mn,Co)_3O_4$ spinels used for protective coatings, $MnCo_2O_4$ and $Mn_{1.5}Co_{1.5}O_4$ are the most widely studied [13,26–32]. The first one is a pure cubic spinel whereas the second one at room temperature is a mixture of tetragonal Mn_2CoO_4 and cubic $MnCo_2O_4$ [23,33]. These materials were shown to successfully block Cr diffusion and protect fuel cell cathodes from the degradation [13]. During long time exposure at ~800°C iron might also diffuse from steel to the coating. To mitigate the transport and for improved TEC matching, iron doped spinel has also been proposed as an alternative [34,35]. Also effects of Cu, Ce, Ni substitutions were studied to increase the electrical conductivity and thermal expansion coefficient match [36–38].

In the literature many methods for fabrication of protective coatings were reported, including sol-gel [30], spraying process (including plasma processes) [39], slurry coating [32], screen-printing [40], electrophoretic deposition [41–44], thermal evaporation [33] and finally electroplating [45]. These methods result in different microstructures of the as-prepared coatings and require different level of post application processing. To improve the density of the coatings, either mechanical compaction [16] or reduction firing (reactive sintering) [22,46] was proposed. When exposed to a reducing atmosphere, the spinel decomposes to MnO and metallic Co. Upon reoxidation it reforms a spinel again with a denser microstructure . This approach has been commonly used with some success.

Promising tests on a laboratory level resulted in transfer to the prototype stage by several groups. Several stack tests performed with the use of $(Mn,Co)_3O_4$ based spinels have proven its feasibility as a coating that can ensure long-term stability of large stacks. In a 2.5 kW stack test including 18 repeating units, 100 μm thick iron doped spinel deposited by atmospheric plasma spraying on Crofer 22 APU proved impermeable to Cr over > 6000 hours test period at temperature below 800°C [47]. Also other stack tests performed at FZ Jülich on $(Mn,Co,Fe)_3O_4$ spinel coated Crofer 22 APU interconnects result in low stack degradation rates holding promise for future commercialization.

[48–50]. These studies in full scale stacks at technologically relevant operation conditions clearly shows the potential of the Mn,Co spinels as interconnect coating material.

Summarizing results obtained so far, manganese-cobalt spinels have been proven successful as protective coatings both in research and in real stack operation (when considering T < 850°C operation). Relatively thick and dense layers of spinels prepared by plasma techniques are proving that these materials can be used over long times with very low degradation rates. To reduce cost and facilitate manufacture it is of relevance to investigate alternative fabrication routes of such coatings.

In this work a novel processing route for preparing coatings of $MnCo_2O_4$ and $MnCo_{1.9}Fe_{0.1}O_4$ is presented. First the synthesis of phase pure material is presented, then preparation of mechanically stable protective coatings with use of an infiltration step is introduced. Prepared coatings are analyzed by measuring the area specific resistance at 750°C over a 5000 hours ageing experiment. Finally, results of microstructural analysis prior to and after the ageing test are reported.

Experimental

For preparation of the coatings, appropriate spinel powders were produced by a modified Pechini/polymeric precursor method [51]. In this work spinel powders of $MnCo_2O_4$ (abbreviated as MCO) and $MnCo_{1.8}Fe_{0.2}O_4$ (abbreviated as MCFO) were prepared. Nitrates of Mn, Co and Fe (hydrated nitrates, Sigma Aldrich, USA) were dissolved in 99.9% ethanol. Then ethlyene glycol and citric acid were added during continuous stirring on a hot plate. This solution was then further stirred with simultaneous heating at 80°C for around 48 hours. During this time ethanol evaporates and metal cations form chelates with ethylene glycol and citric acid. Part of this solution was used later to impregnate the coating. Next step in the preparation of the powder was raising the temperature in steps: first to 130°C and then 150°C to form a solid gel/resin. Afterwards the gel was calcined/pyrolised at 400°C in a muffle furnace. The calcined material was further heat treated at 800°C to fully crystallize spinel powders.

Coatings were prepared in two steps, resembling the methodology presented in [51]. First a porous scaffold of the spinel was prepared on the cleaned steel. Later, this porous matrix was infiltrated with the equivalent solution, containing the same metal nitrates as used previously to prepare the spinel powders.

The porous scaffold coatings for later impregnation were prepared by a simple brush painting method on both sides of the alloys. Pastes were prepared by mixing powders with ethylene glycol plus addition of a binder (ESL403, Electroscience, USA). Mixing was performed in an agate mortar. Crofer 22 APU (Thyssen Krupp VDM, Germany) plates with thickness of 1.5 mm, was laser cut to dimensions of 40 x 20 mm^2. Only the central part of 2 x 2 cm^2 was painted as an active area on both sides of the alloy. Crofer 22 APU was used in the as-received state, only cleaned in ethanol and acetone in an ultrasonic bath prior to use. Alloy samples were weighed in order to control weight (thus thickness) of the painted coatings. For each spinel material two thicknesses of the coatings were prepared. Approximately 30 µm and 50 µm thick coatings were obtained (as observed later by cross-section microscopy analysis). After painting the samples were left for 15 minutes to level off the paste at room temperature and then dried at 50°C and subsequently at 130°C. Final removal of ethylene glycol and binder residues took place via calcination at 400°C in air.

The as-prepared samples were used for the infiltration of the same material into the porous matrix. To lower the viscosity of the solution used for the infiltration, it was first mixed 50:50 by volume with butoxyethanol. In order to infiltrate coatings, several drops of the solution were placed on top of the coating and left to penetrate its volume. After drying at 50°C and 80°C the samples were heat treated at 400°C. This formed a single infiltration procedure. Impregnation procedure was repeated in total 10 times.

For qualitative analysis of the obtained powders, x-ray diffractometry (XRD) was used. Patterns were collected at room temperature using a Bruker D8 Advance apparatus with Cu Kα radiation and a LynxEye detector in a standard 2θ configuration.

A JEOL JEM-3000F transmission electron microscope (TEM), operated at 300 kV and equipped with a field emission gun, was employed to characterize the prepared powders, which was carefully scratched from the targeting surface of samples. The point resolution is 0.19 nm. An energy dispersive X-ray spectroscopy (EDS) microanalysis detector was used to conduct chemical analysis of samples.

For the electrical characterization of the coatings at high temperatures, a specially designed measurement rig using a clam shell furnace was used. It allows for the measurement of the electrical resistance across the growing chromia layer, which is represented by the Area Specific Resistance. A schematic drawing of the rig is shown in Figure 3A. It allows for a simultaneous measurement of several samples with separate measurement of both coated sides (interfaces) for all samples. One single repeating unit consists of the coated Crofer 22 APU sample with spot welded platinum wire and two contacting ceramic plates facing the coating in the 2 x 2 cm^2 active area. Another platinum wire is placed in between neighboring ceramic plates. These contacting plates are made from $La_{0.85}Sr_{0.15}MnO_3$ (LSM) ceramic by a slip casting process. LSM plates are in porous bisque state and their cross-plane resistance in the setup is measured separately for reference. For improved electrical contact between the LSM plate and the measured surface, a LSM contact layer is sprayed on the LSM plates. This is necessary to ensure good contact with reproducible properties over a large surface area [52,53]. In this setup, a single voltage drop (single interface) is measured across the alloy and the contacting plate. The corresponding resistance includes the resistances of the alloy plate, the oxide scale, the coating, the LSM plate, and relevant interfaces between them. This setup closely resembles the situation in a real SOFC/SOEC stack, where contacting pastes are often applied [54–57]. On top of the samples arranged for the ASR measurement, an alumina block is placed and a mechanical load of 8 kg (corresponding to 0.2 MPa load) is applied. An electrical current equal to 0.5 A cm^{-2} was passed through the stack to allow determination of the interface resistances. The current value was measured by use of a reference resistance for which a voltage drop was logged.

Temperature of the samples was monitored by two thermocouples (TC1 and TC2 in Figure 3A) placed few millimeters away from the samples.

After arranging the samples and connecting all wires to terminals of the data logging system, the furnace was heated to obtain a temperature of 750°C next to the samples. The heating rate was 60 °/h. The electrical current was turned on at a temperature of 400°C. After 5000 hours of aging at 750°C, thermal cycling between 750°C and room temperature was performed. In order to accurately measure the resistance as a function of temperature for the calculation of the activation energy, first a cooling step was performed with a ramp rate of 10 °/h. Afterwards, heating and cooling were performed with a ramp rate of 120 °/h. Current was flowing at all times during temperature ramping.

After the final cooling down, the samples were removed from the rig and embedded in epoxy (EpoFix, Struers, Denmark) for the preparation of samples suitable for electron microscopy. During the long-term exposure the entire stack sintered together and remained a single block. Final polishing step was performed with a 0.2 µm diamond polishing paste. Before microscopy analysis the sample surface was sputtered with carbon to avoid surface charging during the analysis.

Scanning electron microscopy (SEM) images were taken using a Zeiss Supra 35 FEG-SEM and a table top Hitachi TM3000 equipped with energy dispersive X-ray analyzers (Noran and Bruker, respectively).

Results and discussion

Fabrication of manganese-cobalt spinel powders was the first task in this work. For both compositions ($MnCo_2O_4$-MCO and $MnCo_{1.8}Fe_{0.2}O_4$-MCFO), around 50 grams of powders were produced in a single step. Phase purity of the powders was checked by x-ray diffractometry. Both the powders after the first calcination step at 400°C and the one after final heat treatment at 800°C were analyzed.

Measured diffractograms are shown in Figure 1A. Already after heat treatment at 400°C the spinel phase is formed. Broad peaks indicate very small crystallite size. In the case of the MCO powder, several peaks can be clearly ascribed to the tetragonal spinel phase (ICDD card number 77-471). In the case of MCFO, peaks are very broad so a clear differentiation between possible different spinels is difficult, however no clear peaks from secondary phases are observed. After the second heat treatment step at 800°C, only a pure cubic spinel phase (ICDD card numer 23-1237) is detected for both materials with no sign of other phases being present.

The possible presence of other spinel phases might not be detrimental to its protective action, as similar compositions are also used as protective coatings for the interconnects. In addition to the $MnCo_2O_4$ composition synthesized in this work, another composition, $Mn_{1.5}Co_{1.5}O_4$, is also widely studied, which is actually a mixture of cubic and tetragonal phases at room temperature.

For the powder analysis transmission electron microscope was also used. Figures 1B and 1C show the morphology of the synthesized particles. The particle size of both the materials is estimated to be around 250 nm. The characteristic crystal planes were identified by the high-resolution TEM images. On the powders also a compositional analysis by EDS was performed to check the cation content in the materials. For the MCO powder, the cation content (at.%) was 33.9 and 66.1 for the Mn:Co, thus the ratio is 1.95 and close to the nominal one. For the MCFO, the cation content (at.%) was 33.2:5.3:61:5 for the Mn:Fe:Co respectively. The ratio of the B site cations (Co+Fe) to the A site is 2.01. The ratio of Fe to Co content is 0.09, so also close to the desired composition.

Thus, as concluded by the x-ray diffractometry and transmission electron microscope analysis, the modified Pechini method is well suited to produce phase pure powders with the desired composition and crystallite size (~250 nm).

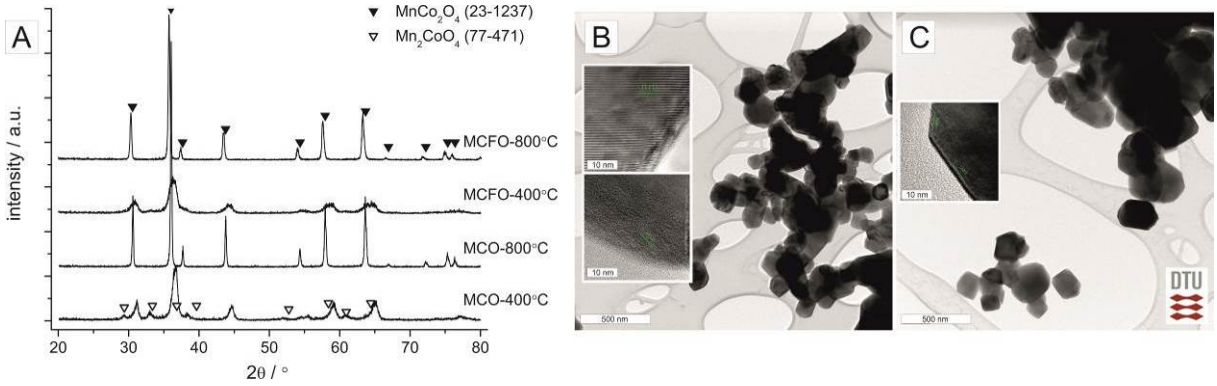

Figure 1. A) X-ray diffractometry patterns of $MnCo_2O_4$ and $MnCo_{1.9}Fe_{0.1}O_4$ powders after heat treatment at 400°C and 800°C and high-resolution TEM images of the B) MCO and C) MCFO powders prepared by a modified Pechini method and calcined at 800°C.

Cross section and surface images of the as-prepared, painted and impregnated MCFO coating on the Crofer 22 APU steel are shown in Figure 2. The thickness of the coating is around 30 µm. The coating is relatively porous. In the high magnification images, surface views of the non-impregnated and impregnated coatings are shown. The grain size of the MCFO material is around 250 nm. After the impregnation, some degree of densification occurs. Grains are much better connected which is important for its electrical conductivity and mechanical integrity. The grains of the impregnated phase are smaller than ~5 nm. So in the case of the initially produced powders (used for initial XRD characterization shown in Figure 1A), the respective grain size for a powder processed at 400°C was 5 nm and grew to 250 nm after processing at 800°C.

Protective layers developed in this work are not sintered at high temperature or by the reduction sintering method prior to characterization. Before the impregnation, coatings are very easily destroyed and spall off readily. After the impregnation and heat treatment however, grains are well connected and mechanical properties allow for safe handling of the samples.

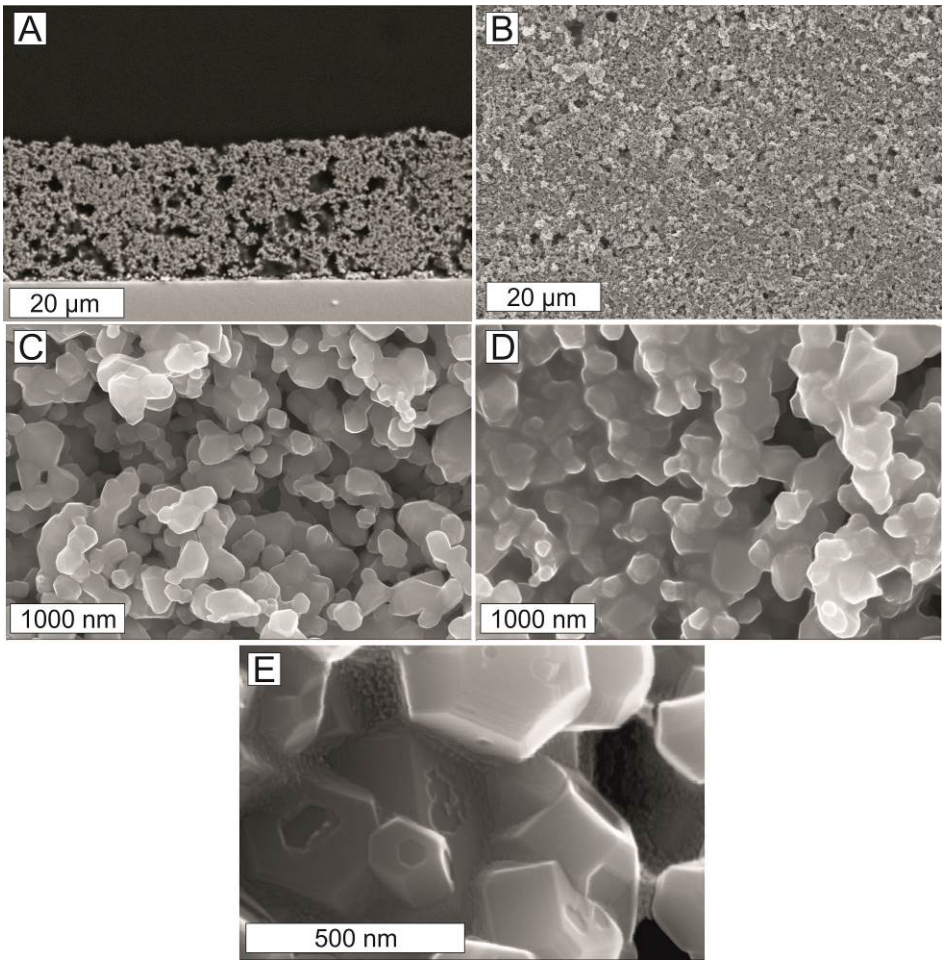

Figure 2. SEM images of the prepared coatings, cross-section (A) and surface of the impregnated coating (B,D,E). Also shown surface of the coating without impregnation (C).

The as-prepared samples, coated either with $MnCo_2O_4$ or $MnCo_{1.8}Fe_{0.2}O_4$ and with two thicknesses (30 µm and 50 µm) for each composition were tested electrically at 750°C for the evaluation of the area specific resistance (ASR) under a current load of 500 mA cm^{-2}.

Figure 3B and 3C presents a continuous ASR measurement for selected, representative samples. Also a value measured for the auxiliary LSM contact plate is shown. It is observed that after the initial 500 hours with a relatively rapid ASR increase rate, all coated samples behaved very similarly with a slow increase of the ASR over time (the rate of degradation decreases over time). The un-coated Crofer 22 APU sample shows an initial decrease of the ASR lasting also around 500 hours and then a steady increase with a higher rate than for all the coated samples.

At 1000 hours, the setup was cooled down unintentionally. It was subsequently heated up again to 750°C. This unplanned temperature cycle had only a minor effect on the ASR of the coated samples and a slightly larger effect on that of the contacting plate. The lowering of the ASR values after this thermal cycle might be due to improved contact after stresses relaxation during the cycle.

As can be seen in Figure 3B, the ASR level of the LSM contact plate is around 10 mΩ cm^2 and is decreasing steadily over time. The plates were initially not sintered and were used in a bisque sintered state in the setup. A slow sintering process takes place during the measurement, which results in an increasing electrical conductance.

Area Specific Resistance calculated in this work are represented by two values: $ASR_{(TOTAL)}$, which includes the oxide, coating and LSM plate resistances, and $ASR_{(TOTAL-LSM)}$, where the resistance of the LSM plate has been substracted based on the in-situ measurement of the resistance of one such plate.

The measured $ASR_{(TOTAL)}$ for all coated samples is around 15 mΩ cm^2. This value contains the resistance of the steel (which is negligible), the oxide scale, the coating, the LSM contacting plate, and all the interfaces. Taking into account the ASR of the contact plate and subtracting it from the ASR values obtained for the samples, the ASR of the pure oxide/coating is much lower (Figure 3C) ~5 mΩ cm^2. There is usually a small scatter between the starting levels of the ASR for all samples, values lie between 10 mΩ cm^2 and 15 mΩ cm^2. This is believed to originate from the LSM plate with the sprayed LSM contact layer, which can either be slightly misaligned or with different thickness. For the long-term performance evaluation, the starting ASR value is small and behavior is dominated by the increase due to oxide scale growth. The most conservative evaluation will be to compare the absolute rate of increase of the ASR (expressed as δASR/1000h) over time.

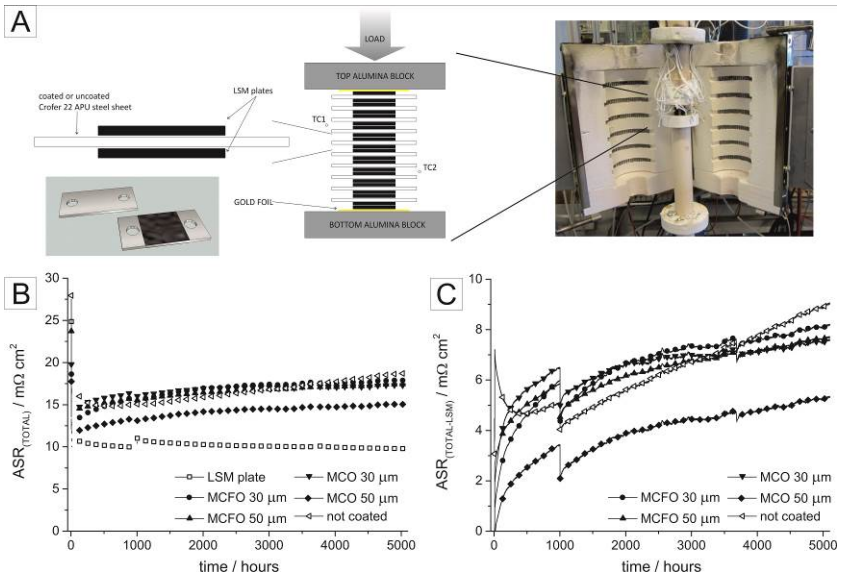

Figure 3. A) Schematic drawing of the area specific resistance measurement setup and plots of ASR as a function of time during oxidation at 750°C: B) ASR including the LSM plate contribution is plotted, whereas in C) ASR with subtracted contribution from the LSM plate is plotted.

From the average increase of the ASR observed between 2000 and 5000 hours, the degradation rate of ASR, for both $ASR_{(TOTAL)}$ and $ASR_{(TOTAL-LSM)}$ was calculated assuming a linear behaviour. Obtained ASR values are included in Figure 4. All the coated samples show very similar degradation rates. The thickness and the material composition does not influence the degradation rates. For $ASR_{(TOTAL)}$, all coated steels are characterized by a degradation rate close to 0.3 mΩ cm^2 per 1000 hour. Uncoated Crofer 22 APU has an ASR increase rate of 1.1 mΩ cm^2 per 1000 hour, which is almost 4 times higher. The results show that all the coatings studied in this work have a very positive effect on reducing the ASR degradation.

The observed degradation rates can be caused mainly by a slower growth of the poorly conductive chromium oxide at the interface between the alloy and the coating. The conductivity of this oxide layer is expected to be in the order of few mS cm^{-1}. For comparison, the electrical conductivity of the MCO and MCFO are around 60 S cm^{-1}; so around 4 orders of magnitude higher. In case of the uncoated samples, the contacting of the steel with the LSM contacting plate will influence the

growth of the oxide scale, as the LSM has been reported to have a positive effect on corrosion protection [20,58].

Using the ASR increase rate values and assuming a simple linear extrapolation, ASR values after 40000 hours of operation can be estimated. The ASR increase could be expected to follow a parabolic behaviour, hence a linear extrapolation is a “worse case scenario” approximation – it will yield higher values than the more realistic parabolic extrapolation. Here, the resulting ASR has been calculated after 40000 hours for the $ASR_{(TOTAL-LSM)}$ values. Taking the initial ASR value of 2-5 mΩ cm^2, the ASR after 40000 hours will reach ~20 mΩ cm^2 for coated samples and up to 55 mΩ cm^2 for the uncoated ones. If one would use the $ASR_{(TOTAL)}$ for the calculation, results would be roughly the same, as lower ASR increase rate is offset by higher starting value (10-15 mΩ cm^2), thus yielding very similar estimates (27 and 59 mΩ cm^2 for coated and uncoated respectively). Used data extrapolation method does not take into account possible effects of a dual atmosphere exposure, changes of gas flows/composition and possible additional thermal cycles and thus should be treated only as a limited approximation.

From the measurements presented here, it is thus clear that spinel coatings without a reduction sintering step can be effective in reducing the resistance increase with time over the thermally grown oxide scale over long time (>5000 hours) including thermal cycling. In general, these results are applicable for both the fuel and electrolysis cell mode operation (reversed current direction). No difference in the ASR development has been noticed for the two studied interfaces of each sample, as opposed to some other research [59–61]. One possible explanation for the lack of the difference might be relatively low current density used in this work (500 mA cm^{-2}).

Prepared coatings effectively improve electrical performance of the alloy allowing for a lower ohmic resistance and thus losses caused by the oxide scale growth. It must be noted that this setup evaluates only ohmic resistance changes, possible adverse/beneficial effects of the coatings on electrode polarization when placed next to an operating cell was not evaluated.

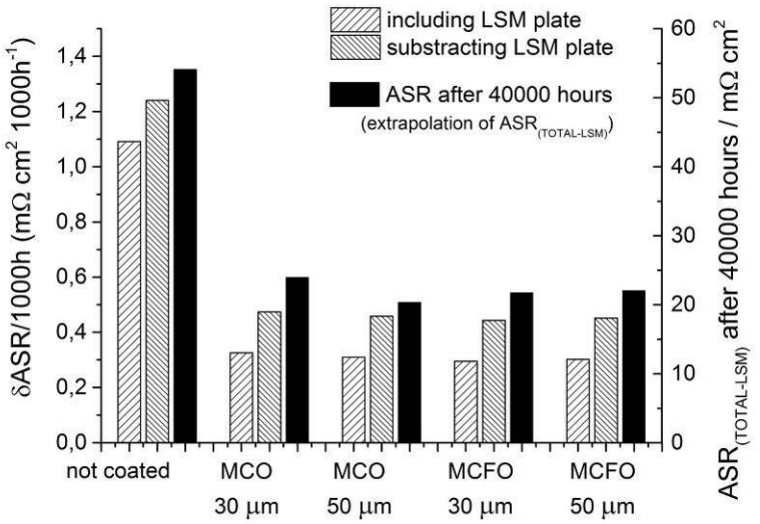

Figure 4. Comparison of ASR increase rates for coated and uncoated samples.

After the 5100 hours of isothermal aging, thermal cycling between 750°C and room temperature was performed (the samples also underwent one unintended thermal cycle after 1000 hours of operation). The ASR changes during the last five cycles for a representative sample are presented in Figure 5A. Cooling to room temperature and heating up back to 750°C had no effect on the ASR of any of the samples at 750°C. This shows that neither in the coating nor in the formed oxide scale severe cracking occurs. The resistance value at room temperatures is 5 orders of magnitude higher than at 750°C reflecting the thermal activation of the charge transport through the oxide scale (believed to dominate the electrical response).

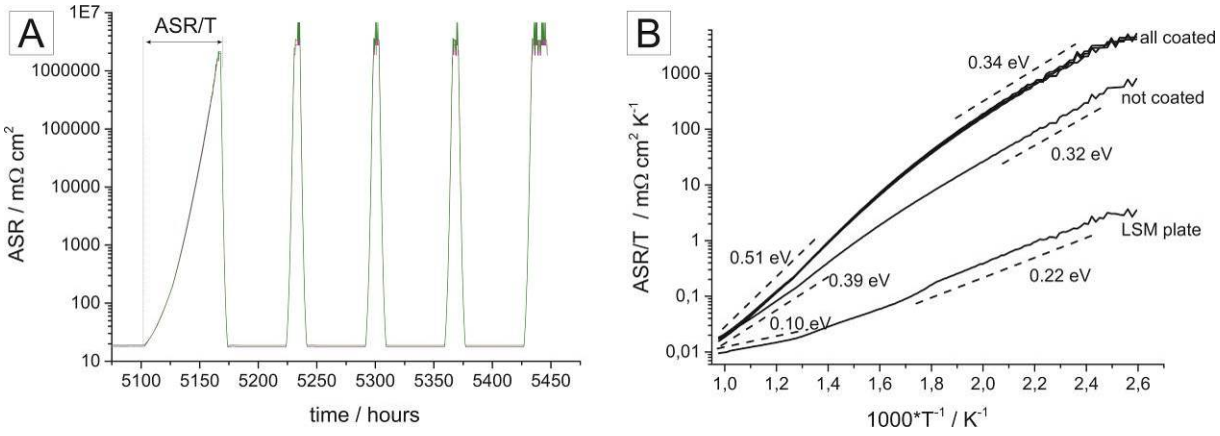

Figure 5. Plot of ASR values for MCO sample A) during thermal cycling between 750°C and room temperature and B) as a function of the inverse of temperature.

From the dependence of the Area Specific Resistance on the inverse of the temperature, the activation energy, E_A, of the effective electrical conductivity can be calculated. In this case an Arrhenius type equation is fitted to plots as shown in Figure 5B (with ASR being proportional to the inverse of σ):

$$\sigma T = \sigma_0 \exp\left(-\frac{E_A}{k_B T}\right) \Rightarrow \frac{ASR}{T} = \frac{\sigma}{\sigma_0}\exp\left(\frac{E_A}{k_B T}\right) \qquad \text{[Equation 1]}$$

where: σ – electrical conductivity [S cm^{-1}], σ_0 – pre exponential constant [S cm^{-1}], E_A – activation energy [eV]. k_B – Boltzmann constant [eV K^{-1}] and T – temperature [K].

A plot of the ASR values as a function of the temperature for all the coated samples and the LSM contact plate during the first slow cooling cycle after 5100 hours is shown in Figure 5B. According to Equation 1, the slope of the curves is proportional to the activation energy.

For all the samples, activation energies for the high temperature and the lower temperature region are noticeably different. All the coated samples follow exactly the same behaviour. In the high temperature region (between 550°C and 750°C), the activation energy is 0.51 eV, while in the lower temperature range (between 500°C and 200°C) it is ~0.34 eV. For the un-coated sample, the activation energies are 0.39 eV and 0.32 eV for the high and the low temperature region,

respectively. In the lower temperature region, the activation energy for both the coated and the uncoated samples is relatively similar whereas they differ at high temperatures. The activation energy measured for the LSM contact plate is much lower, being 0.10 eV and 0.22 eV in the high and low temperature region respectively. In the lower temperature range, some measurement noise is visible, that might be due to very low current and high resistance, also with a Joule heating contributing to the noise. Values obtained for the spinel coated samples agree with the values reported in the literature. For pure spinels in the form of sintered pellets, activation energy of ~0.45 eV has been reported [62], whereas if deposited as a coating, 0.70 eV has been reported by Kruk et al. [40]. It was similar (0.67 eV) to uncoated samples suggesting the same mechanism of electrical conduction or rather that part of the oxide scale/coating that dominate the resistance is the same. In some other studies, the activation energy of Mn,Co spinels has been measured to be ~0.2 eV, whereas activation energies for Cr_2O_3 and Mn,Cr spinels have been reported to be 0.51 eV and 0.44 eV respectively [63]. The ASR measured here is the sum of the thermally grown chromia scale, the reaction layer (spinel structure) and the coating. Evidently, the composition differences between coatings and the thickness of the coating do not affect the measured ASR, indicating that this is dominated by the chromia scale and possibly the reaction layer. The grown scale as well as the reaction layer are thus electrically very similar between the four coatings. Whereas the coated samples differ from the uncoated sample, reflecting that certainly the electrical properties of the spinel type reaction layer differ and possibly also the properties of the chromia below the reaction layer. The electrical properties of chromia is highly dependant on minute amounts of foreign impurity cations dissolved in the structure and reported conductivities of chromia consequently show a large scatter [64].

The electrical performance of the coatings is only one important factor for stack performance. Another contribution to the stack degradation is chromium poisoning of the SOFC/SOEC oxygen electrodes [65,66]. At high pO_2, in the presence of steam, chromium can form volatile species that can react with the cathodes lowering their electrochemical performance [67,68]. Chromium diffusion

and the chromium retention capabilities of the coating can to some extent be assessed by the post-mortem microstructural analysis of the cross sections.

Post mortem analysis:

Cross section images of the MCO coated and uncoated Crofer 22 APU after the ASR measurement are shown in Figure 6. All coated samples had very similar microstructure. Also both sides of all samples were very similar, i.e. current flow direction had no noticeable effect on the oxide formation or on the coating microstructure after the test. In Figure 6 A-C several interesting features are visible. The coatings have densified near the oxide interface, forming a 2-3 µm thick, continuous and dense layer. This reaction layer is very beneficial for corrosion protection as it significantly retards chromium diffusion from the chromia scale to the coating and further out. Chromia on coated samples, as visible in Figure 6C, is around 1 µm thick after 5300 hours at 750°C. This thickness after a relatively long measurement time can be regarded as satisfactory and far from possible scale breakdown/spallation due to mechanical stresses [69,70].

Pronounced “internal” corrosion occurred in many places beneath the surface oxide scale. In addition to the normally present TiO_2 internal oxides, visible as evenly distributed small spots up to a depth of 8 µm from the oxide scale – steel interface, large internal oxide with diameters in the range of 2-4 µm are noticed. These internal oxidation products are distributed almost across the entire cross section and are present in all coated samples. They are observed 1 µm beneath the chromia and are observed on both sides of the coated samples. These oxides have a $MnCr_2O_4$ stoichiometry and their presence has been reported previously on MCO coated Crofer 22 APU [71].

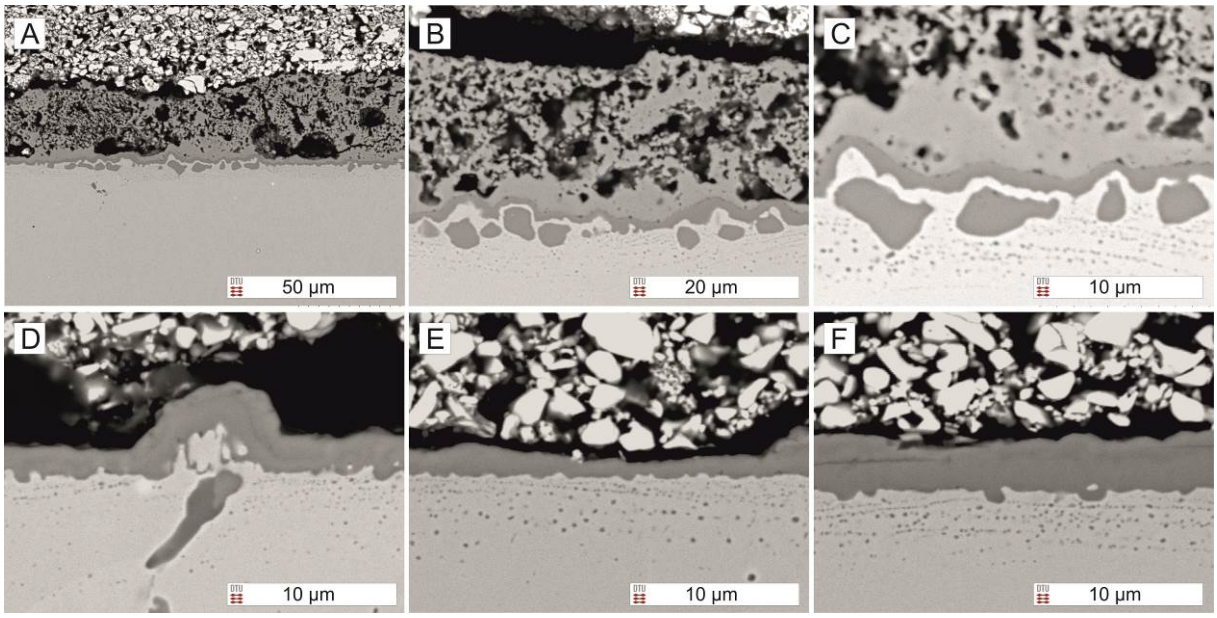

Figure 6. SEM images of oxidized MCO coated samples (A-C) and uncoated steel. Pictures from three different locations are reproduced to illustrate the variation of thickness (D-F).

In Figure 6D-F, cross sections of the uncoated Crofer 22 APU sample are reproduced together with the LSM particles from the contacting plate. Here, oxide scale is evidently thicker than on the coated samples with a varying thickness between 2 to 4 µm, shown in Figure 6E and 6F. Small TiO_2 internal corrosion products are also visible but there are only few spots with larger internal corrosion products present. This happens for a normal Crofer 22 APU typically along grain boundaries. The shape of these particles is however different from the internal oxides present in the coated samples. By comparison of the coated and uncoated samples, a beneficial effect of the MCO and the MCFO spinel on lowering corrosion rate is noticed: the thermally grown oxide scale (chromia) on the uncoated sample is 2-3 times thcker than on the coated samples. This results in a considerable improvement in the expected lifetime of the interconnect.

In addition to electrically limited lifetime, another requirement to the interconnect is given by mechanical properties of the steel/oxide/coating structure [72,73]. Due to differences in thermal expansion coeficient of different layers, thermal stresses will arise during heating and cooling, and when some critical thickness is reached, it will lead to cracking or delamination of the scale. The risk

of mechanical failure in the scale in a simple model increase in direct proportion to the scale thickness as the elastic energy stored in the scale, either due to growth stresses or due to TEC mismatches, is proportional to oxide thickness.

Taking into account oxide thickness measured on the coated and oxidized samples (~1 μm) and the oxidation time (5500 hours), the corrosion rate can be approximately calculated (assuming Wagner-type behavior: $h^2 \sim k_p t$, where h – oxide thickness, k_p – corrosion rate, t – oxidation time). Although this should be calculated based on several points measured over time, here it will be used only for some rough estimations. This corrosion rate, can be used to estimate the expected oxide thickness after 40000 hours of operation. Thus calculated thicknesses are ~3 μm after 40000 hours operation at 750°C (compared to 1 μm after 5500h). This thickness is acceptable from the mechanical point of view, it should not cause any problems with cracking and delamination of the oxide scale, as interface toughness is expected to be able to withstand possible energy releases from detaching a scale of this thickness (given the TEC mismatch). Also well adhering scales up to much higher thicknesses ~6-8 μm have indeed been observed on Crofer 22 APU when oxidized at higher temperatures [12,74].

Elemental analysis maps for O, Cr, Co, Mn and Fe, obtained by energy dispersive x-ray analysis of the MCO coated sample together with a SEM image are shown in Figure 7. In comparison to the coating, oxygen concentration is visibly higher in the internal oxide and the oxide formed on the steel/coating interface. Chromium rich oxide is visible in this interface, however the chromium concentration is lower in the internal oxides. Almost no chromium is detected in the coating. Integrated area analysis of the coating have shown a maximum of 0.5 at.% Cr in the coating, however this is within the EDS detector error. Point analysis of the coating, has shown that the composition of the coating after the test is: Co/Mn/O/Cr/Fe : 30.3/17.2/51.4/0.4/0.8 at.% respectively. In comparison the starting powder and the as-prepared coating, the spinel got enriched in Mn. The ratio of Co to Mn is now 1.76, instead of the initial value of 2. It might point to the diffusion of Mn either from the steel or from the

LSM contact layer. The densified coating next to the interface has the same composition as the rest of the coating, no excessive reaction with chromium and manganese has been detected (within detection accuracy of the EDS). The iron map shows clearly the spots of the internal oxidation products, which contain no iron. On the base of the obtained EDS results, it is confirmed that a 2-4 µm thick dense reaction zone contains less than 1 at.% Cr and thus reduces outward Cr diffusion at these conditions.

In case of a pure Co spinel (with LSM layer on top) used on the Crofer 22 APU [75], also a dense reacton layer is observed, but it was observed to be enriched both with manganese and chromium (~10 at.% of Cr and ~8 at.% Mn). Presence of chromium in this reaction layer causes further outward diffusion of chromium to the surface and this coating is likely to be less protective towards Cr-poisoning of the electrodes. By adding manganese to the cobalt spinel, formation of a more protective coating is achieved.

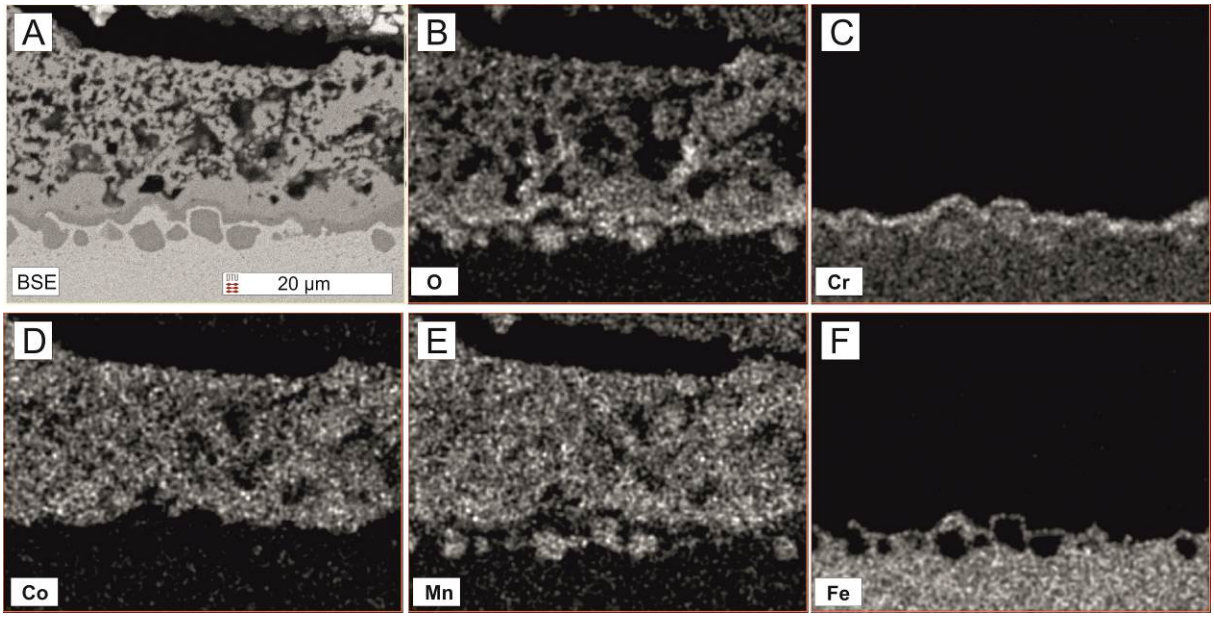

Figure 7. SEM (A) and EDS (B-F) elemental analysis of MCO sample after 5300 hours of oxidation at 750°C.

Based on the performed EDS analysis on the coated samples, it is shown that the initially relatively porous spinel coating densified next to the oxide/steel during the high temperature exposure (750°C) and succesfuly blocked chromium outward diffusion. The results presented in this work indicate that the deposition method does not play a crucial role in the preparation of spinel coatings. By formation of a dense reaction layer, when in contact with the oxide or the alloy, a spinel has a tendency to densify by itself and form a protective and well conducting layer of very low Cr permeability. For the here applied preparation method, the high temperature sintering and/or reduction steps can be omitted thus reducing production costs for coating of interconnects. As described by Akanda et al. [76], the reduction treatment in the fabrication of the spinel coated interconnects contributes with ~20% of the overall coating cost. Additionally, no influence of thickness has been found in this work; increasing thickness from 30 µm to 50 µm makes no difference in protective behavior. The presence of a porous but highly reactive layer that can udergo reaction and densification is enough to provide a protective action on the interconnect as deemed based on the quantities here evaluated.

The formation of the Mn,Co reactive layer is schematically presented in a simplified model in Figure 8. The initially porous coating deposited on the steel after heat treatment (oxidation) densifies on top of the chromia scale. In the early stage of oxidation, reaction layer forms simulatenously with chromia. It must draw Mn and Co from the porous coating and Mn from the steel. This reaction layer, when formed, strongly retards outward chromium diffusion protecting the porous coating and other layers. Up to 1 at.% of Cr can be found in the reaction layer after the long exposure time. Similar model has been presented by Magdefrau et al. [71]. In their case, the reaction layer contained large amount of Cr (after 1000 hours at 800°C Mn/Co/Cr ratio was 7/4/3) and was being continously enriched in Cr, forming a mixed Mn,Co,Cr spinel with low electrical conductivity. In our case, only ~1 at.% of Cr diffuses into Mn,Co reaction layer after ~5000 hours. Formation of this dense reactive layer with low Cr content is essential for ensuring protective properties of initially porous coatings.

Development of the dense and protective Mn,Co spinel layer might be dependent on initial microstructure, grain size and thermal treatment. In this work prepared layers were quite porous, but with small grain size and additionally were impregnated, which created nanoparticles of the spinel. We believe that the presence of the nitrate precursors of Co and Mn improve the formation of a dense spinel layer at the steel-coating interface. Unfortunately, samples with no infiltration of the nitrates were too fragile to include them in the experiments, thus no direct comparison could be made in this study.

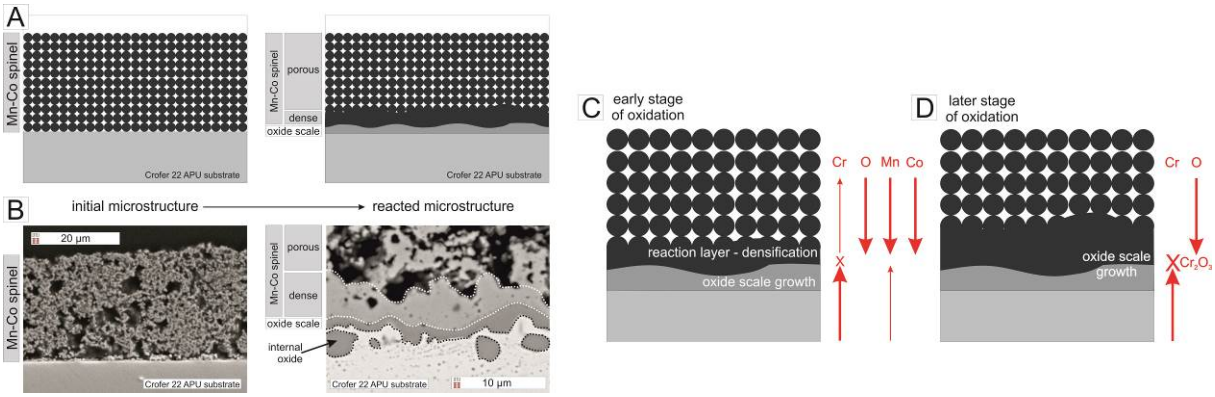

Figure 8. Schematic presentation (A) and micrographs (B) of formation of the reactive layer and (C-D) fluxes of ions across the substrate/oxide/reaction layer/coating.

Conclusions

In this work $MnCo_2O_4$ and $MnCo_{1.8}Fe_{0.2}O_4$ protective coatings were prepared on Crofer 22 APU steel. Two coating thicknesses were analyzed (30 µm and 50 µm). The fabrication of the coatings was based on firstly preparing a porous matrix and then impregnation with the coating precursor, expected to increase sintering activity/reactivity such that a high temperature densification step could be avoided. Coatings were tested electrically for 5300 hours at 750°C.

All coated samples show very similar behavior: there are no effects of composition nor thickness on the protective action as evaluated by the ASR increase and from post-mortem micrographs. The ASR of the coated samples increases ~4 times slower than for the uncoated sample. Starting from

~15 mΩ cm^2, the average rate of increase for the coated samples was ~0.3 mΩ cm^2/1000h. Neither the composition nor the thickness of the protective coating had a measurable influence on electrical conductivity. Assuming a linear increase of the ASR over time, obtained results would allow 40000 hours operation with the final ASR level well below 30 mΩ cm^2.

Post mortem analysis shows, that though the coatings were initially very porous, they densified near the thermally grown oxide interface. A dense, 2-4 µm thick layer was formed that blocked or at least retards very significantly outward chromium diffusion. Only a very small amount of chromium (~0.5 at.%) can be found in the coating after ~8 months oxidation. The spinel coating also slowed down the formation of the chromia scale. Its average thickness for the coated samples was between 1 – 2 µm whereas for the uncoated samples the oxide thickness was between 2 – 4 µm. For all of the coated samples, a large amount of internal oxides was found in the steel. In contrast to some reports in literature, we found here that no heat treatment at temperatures significantly above 750°C are necessary to obtain a protective action of the coating.

The results show that even initially porous manganese-cobalt spinel coatings can be highly protective for the steel used as SOFC/SOEC interconnect. They can lower the growth rate of the chromia scale and effectively block chromium diffusion and ensure good electrical properties over prolonged time.

Acknowledgement

Metallographic sample preparation by Ebtisam Abdellahi and Johannes Steen Bang is gratefully acknowledged. Nikos Bonanos is acknowledged for correcting and spell checking the manuscript. DTU is thankful for financial support from Energienet.dk through the ForskEL projects number 2013-1-12013 “Solid Oxide Electrolysis for Grid Balancing” and 2015-1-12276 “Towards solid oxide electrolysis plants in 2020”. GUT acknowledges NCN funded project 2012/05/B/ST7/02153 “New functional layers for solid oxide fuel cells”.

References

[1] Y. Chen, W. Zhou, D. Ding, M. Liu, F. Ciucci, M. Tade, et al., Advances in Cathode Materials for Solid Oxide Fuel Cells: Complex Oxides without Alkaline Earth Metal Elements, Adv. Energy Mater. 5 (2015) n/a-n/a. doi:10.1002/aenm.201500537.

[2] X.-M. Ge, S.-H. Chan, Q.-L. Liu, Q. Sun, Solid Oxide Fuel Cell Anode Materials for Direct Hydrocarbon Utilization, Adv. Energy Mater. 2 (2012) 1156–1181. doi:10.1002/aenm.201200342.

[3] Y. Matsuzaki, I. Yasuda, Electrochemical properties of a SOFC cathode in contact with a chromium-containing alloy separator, Solid State Ionics. 132 (2000) 271–278. doi:10.1016/S0167-2738(00)00654-8.

[4] M.K. Stodolny, B.A. Boukamp, D.H.A. Blank, F.P.F. van Berkel, Cr-poisoning of a LaNi0.6Fe0.4O3 cathode under current load, J. Power Sources. 209 (2012) 120–129. doi:10.1016/j.jpowsour.2012.02.083.

[5] M.K. Stodolny, B.A. Boukamp, D.H.A. Blank, F.P.F. van Berkel, Impact of Cr-poisoning on the conductivity of different LaNi0.6Fe0.4O3 cathode microstructures, Solid State Ionics. 225 (2012) 136–140. doi:10.1016/j.ssi.2012.04.004.

[6] J.W. Fergus, Metallic interconnects for solid oxide fuel cells, Mater. Sci. Eng. A. 397 (2005) 271–283.

[7] W.Z. Zhu, S.C. Deevi, Opportunity of metallic interconnects for solid oxide fuel cells: a status on contact resistance, Mater. Res. Bull. 38 (2003) 957–972. doi:10.1016/S0025-5408(03)00076-X.

[8] I. Antepara, I. Villarreal, L.M. Rodríguez-Martínez, N. Lecanda, U. Castro, A. Laresgoiti,

Evaluation of ferritic steels for use as interconnects and porous metal supports in IT-SOFCs, J. Power Sources. 151 (2005) 103–107. doi:10.1016/j.jpowsour.2005.02.084.

[9] S. Linderoth, P. V. Hendriksen, M. Mogensen, N. Langvad, Investigations of metallic alloys for use as interconnects in solid oxide fuel cell stacks, J. Mater. Sci. 31 (1996) 5077–5082. doi:10.1007/BF00355908.

[10] Y. Larring, R. Haugsrud, T. Norby, HT Corrosion of a Cr-5 wt % Fe-1 wt % Y[sub 2]O[sub 3] Alloy and Conductivity of the Oxide Scale, J. Electrochem. Soc. 150 (2003) B374–B379. doi:10.1149/1.1587726.

[11] P. Piccardo, R. Amendola, S. Fontana, S. Chevalier, G. Caboches, P. Gannon, Interconnect materials for next-generation solid oxide fuel cells, J. Appl. Electrochem. 39 (2009) 545–551. doi:10.1007/s10800-008-9743-8.

[12] Y. Liu, Performance evaluation of several commercial alloys in a reducing environment, J. Power Sources. 179 (2008) 286–291. doi:10.1016/j.jpowsour.2007.12.067.

[13] J. Wu, C.D. Johnson, R.S. Gemmen, X. Liu, The performance of solid oxide fuel cells with Mn–Co electroplated interconnect as cathode current collector, J. Power Sources. 189 (2009) 1106–1113. doi:10.1016/j.jpowsour.2008.12.079.

[14] N. Shaigan, W. Qu, D.G. Ivey, W. Chen, A review of recent progress in coatings, surface modifications and alloy developments for solid oxide fuel cell ferritic stainless steel interconnects, J. Power Sources. 195 (2010) 1529–1542. http://pdn.sciencedirect.com.globalproxy.cvt.dk/science?_ob=MiamiImageURL&_cid=271367&_user=641802&_pii=S0378775309017285&_check=y&_origin=article&_zone=toolbar&_coverDate=15-Mar-2010&view=c&originContentFamily=serial&wchp=dGLbVlt-zSkWb&md5=58abe8f26bcbfa493b8b625cb658c75d/1-s2.0-S0378775309017285-main.pdf.

[15] O. Thomann, M. Pihlatie, M. Rautanen, O. Himanen, J. Lagerbom, M. Mäkinen, et al.,

Development and Application of HVOF Sprayed Spinel Protective Coating for SOFC Interconnects, J. Therm. Spray Technol. 22 (2013) 631–639. doi:10.1007/s11666-012-9880-9.

[16] X. Chen, P. Hou, C. Jacobson, S. Visco, L. Dejonghe, Protective coating on stainless steel interconnect for SOFCs: oxidation kinetics and electrical properties, Solid State Ionics. 176 (2005) 425–433. doi:10.1016/j.ssi.2004.10.004.

[17] S. Molin, B. Kusz, M. Gazda, P. Jasinski, Protective coatings for stainless steel for SOFC applications, J. Solid State Electrochem. 13 (2008) 1695–1700. doi:10.1007/s10008-008-0635-y.

[18] S. Chevalier, J.. Larpin, Formation of perovskite type phases during the high temperature oxidation of stainless steels coated with reactive element oxides, Acta Mater. 50 (2002) 3107–3116. doi:10.1016/S1359-6454(02)00106-4.

[19] M. Palcut, L. Mikkelsen, K. Neufeld, M. Chen, R. Knibbe, P.V. Hendriksen, Efficient dual layer interconnect coating for high temperature electrochemical devices, Int. J. Hydrogen Energy. 37 (2012) 14501–14510. doi:10.1016/j.ijhydene.2012.07.038.

[20] M. Palcut, L. Mikkelsen, K. Neufeld, M. Chen, R. Knibbe, P.V. Hendriksen, Improved oxidation resistance of ferritic steels with LSM coating for high temperature electrochemical applications, Int. J. Hydrogen Energy. 37 (2012) 8087–8094. doi:10.1016/j.ijhydene.2011.11.138.

[21] S. Molin, M. Chen, J.J. Bentzen, P. V. Hendriksen, High Temperature Oxidation of Ferritic Steels for Solid Oxide Electrolysis Stacks, ECS Trans. 50 (2013) 11–20. doi:10.1149/05030.0011ecst.

[22] Y. Larring, T. Norby, Spinel and Perovskite Functional Layers Between Plansee Metallic Interconnect (Cr-5 wt % Fe-1 wt % Y[sub 2]O[sub 3]) and Ceramic (La[sub 0.85]Sr[sub 0.15])[sub 0.91]MnO[sub 3] Cathode Materials for Solid Oxide Fuel Cells, J. Electrochem. Soc.

147 (2000) 3251–3256. doi:10.1149/1.1393891.

[23] Z. Yang, G. Xia, S.P. Simner, J.W. Stevenson, Thermal Growth and Performance of Manganese Cobaltite Spinel Protection Layers on Ferritic Stainless Steel SOFC Interconnects, J. Electrochem. Soc. 152 (2005) A1896–A1901. doi:10.1149/1.1990462.

[24] J.W. Stevenson, Z.G. Yang, G.G. Xia, Z. Nie, J.D. Templeton, Long-term oxidation behavior of spinel-coated ferritic stainless steel for solid oxide fuel cell interconnect applications, J. Power Sources. 231 (2013) 256–263. doi:10.1016/j.jpowsour.2013.01.033.

[25] N.J. Kidner, G. Arkenberg, S. Ibanez, K. Smith, S.R. Akanda, M.M. Seabaugh, et al., Development of Protective Coatings for SOFC Metallic Components, ECS Trans. 57 (2013) 2349–2356.

[26] J.-J. Choi, J. Ryu, B.-D. Hahn, W.-H. Yoon, B.-K. Lee, D.-S. Park, Dense spinel $MnCo_2O_4$ film coating by aerosol deposition on ferritic steel alloy for protection of chromic evaporation and low-conductivity scale formation, J. Mater. Sci. 44 (2009) 843–848. doi:10.1007/s10853-008-3132-x.

[27] M. Yoon, E. Lee, R. Song, H. Hwang, Preparation and properties of a $MnCo_2O_4$ for ceramic interconnect of solid oxide fuel cell via glycine nitrate process, Met. Mater. Int. 17 (2011) 1039–1043. doi:10.1007/s12540-011-6025-5.

[28] Y. Fang, C. Wu, X. Duan, S. Wang, Y. Chen, High-temperature oxidation process analysis of MnCo2O4 coating on Fe–21Cr alloy, Int. J. Hydrogen Energy. 36 (2011) 5611–5616. doi:10.1016/j.ijhydene.2011.01.130.

[29] D.R. Ou, M. Cheng, X.-L. Wang, Development of low-temperature sintered Mn–Co spinel coatings on Fe–Cr ferritic alloys for solid oxide fuel cell interconnect applications, J. Power Sources. 236 (2013) 200–206. doi:10.1016/j.jpowsour.2013.02.058.

[30] A.M. Dayaghi, M. Askari, H. Rashtchi, P. Gannon, Fabrication and high-temperature corrosion

of sol–gel Mn/Co oxide spinel coating on AISI 430, Surf. Coatings Technol. 223 (2013) 110–114. doi:10.1016/j.surfcoat.2013.02.041.

[31] B. Hua, J. Pu, W. Gong, J. Zhang, F. Lu, L. Jian, Cyclic oxidation of Mn–Co spinel coated SUS 430 alloy in the cathodic atmosphere of solid oxide fuel cells, J. Power Sources. 185 (2008) 419–422. doi:10.1016/j.jpowsour.2008.06.055.

[32] Å.H. Persson, L. Mikkelsen, P.V. Hendriksen, M.A.J. Somers, Interaction mechanisms between slurry coatings and solid oxide fuel cell interconnect alloys during high temperature oxidation, J. Alloys Compd. 521 (2012) 16–29. doi:10.1016/j.jallcom.2011.12.095.

[33] L.C. Ajitdoss, F. Smeacetto, M. Bindi, D. Beretta, M. Salvo, M. Ferraris, Mn1.5Co1.5O4 protective coating on Crofer22APU produced by thermal co-evaporation for SOFCs, Mater. Lett. 95 (2013) 82–85. doi:10.1016/j.matlet.2012.12.079.

[34] X. Montero, F. Tietz, D. Sebold, H.P. Buchkremer, A. Ringuede, M. Cassir, et al., MnCo1.9Fe0.1O4 spinel protection layer on commercial ferritic steels for interconnect applications in solid oxide fuel cells, J. Power Sources. 184 (2008) 172–179. doi:10.1016/j.jpowsour.2008.05.081.

[35] X. Montero, N. Jordán, J. Pirón-Abellán, F. Tietz, D. Stöver, M. Cassir, et al., Spinel and Perovskite Protection Layers Between Crofer22APU and La[sub 0.8]Sr[sub 0.2]FeO[sub 3] Cathode Materials for SOFC Interconnects, J. Electrochem. Soc. 156 (2009) B188. doi:10.1149/1.3025914.

[36] B.-K. Park, J.-W. Lee, S.-B. Lee, T.-H. Lim, S.-J. Park, C.-O. Park, et al., Cu- and Ni-doped Mn1.5Co1.5O4 spinel coatings on metallic interconnects for solid oxide fuel cells, Int. J. Hydrogen Energy. 38 (2013) 12043–12050. doi:10.1016/j.ijhydene.2013.07.025.

[37] Y. Xu, Z. Wen, S. Wang, T. Wen, Cu doped Mn–Co spinel protective coating on ferritic stainless steels for SOFC interconnect applications, Solid State Ionics. 192 (2011) 561–564.

doi:10.1016/j.ssi.2010.05.052.

[38] Z. Yang, G. Xia, Z. Nie, J. Templeton, J.W. Stevenson, Ce-Modified (Mn,Co)[sub 3]O[sub 4] Spinel Coatings on Ferritic Stainless Steels for SOFC Interconnect Applications, Electrochem. Solid-State Lett. 11 (2008) B140–B143. doi:10.1149/1.2929066.

[39] J. Puranen, J. Lagerbom, L. Hyvärinen, T. Mäntylä, E. Levänen, M. Kylmälahti, et al., Formation and structure of plasma sprayed manganese-cobalt spinel coatings on preheated metallic interconnector plates, Surf. Coatings Technol. 205 (2010) 1029–1033. doi:10.1016/j.surfcoat.2010.08.030.

[40] A. Kruk, M. Stygar, T. Brylewski, Mn–Co spinel protective–conductive coating on AL453 ferritic stainless steel for IT-SOFC interconnect applications, J. Solid State Electrochem. 17 (2012) 993–1003. doi:10.1007/s10008-012-1952-8.

[41] J. YOO, S.-K. Woo, J.H. YU, S. LEE, G.W. PARK, La0.8Sr0.2MnO3 and (Mn1.5Co1.5)O4 double layer coated by electrophoretic deposition on Crofer22 APU for SOEC interconnect applications, Int. J. Hydrogen Energy. 34 (2009) 1542–1547. doi:10.1016/j.ijhydene.2008.12.005.

[42] H. Abdoli, P. Alizadeh, Electrophoretic deposition of (Mn,Co)3O4 spinel nano powder on SOFC metallic interconnects, Mater. Lett. 80 (2012) 53–55. doi:10.1016/j.matlet.2012.04.072.

[43] F. Smeacetto, A. De Miranda, S. Cabanas Polo, S. Molin, D. Boccaccini, M. Salvo, et al., Electrophoretic Deposition of Mn1.5 Co1.5 O4 on Metallic Interconnect and Interaction with Glass-ceramic Sealant for Solid Oxide Fuel Cells Application, J. Power Sources. 280 (2015) 379–386. doi:10.1016/j.jpowsour.2015.01.120.

[44] D. Szymczewska, S. Molin, V. Venkatachalam, M. Chen, P. Jasinski, P.V. Hendriksen, Assesment of (Mn,Co) 3 3O 4 powders for possible coating material for SOFC/SOEC interconnects, IOP Conf. Ser. Mater. Sci. Eng. 104 (2016) 12017. doi:10.1088/1757-899X/104/1/012017.

[45] J. Wu, C.D. Johnson, Y. Jiang, R.S. Gemmen, X. Liu, Pulse plating of Mn–Co alloys for SOFC interconnect applications, Electrochim. Acta. 54 (2008) 793–800. doi:10.1016/j.electacta.2008.06.057.

[46] Z. Yang, G.-G. Xia, X.-H. Li, J.W. Stevenson, (Mn,Co)3O4 spinel coatings on ferritic stainless steels for SOFC interconnect applications, Int. J. Hydrogen Energy. 32 (2007) 3648–3654. doi:10.1016/j.ijhydene.2006.08.048.

[47] Q. Fang, L. Blum, P. Batfalsky, N.H. Menzler, U. Packbier, D. Stolten, Durability test and degradation behavior of a 2.5 kW SOFC stack with internal reforming of LNG, Int. J. Hydrogen Energy. 38 (2013) 16344–16353. doi:10.1016/j.ijhydene.2013.09.140.

[48] L. Blum, L.G.J. (Bert) de Haart, J. Malzbender, N.H. Menzler, J. Remmel, R. Steinberger-Wilckens, Recent results in Jülich solid oxide fuel cell technology development, J. Power Sources. 241 (2013) 477–485. doi:10.1016/j.jpowsour.2013.04.110.

[49] L. Blum, P. Batfalsky, Q. Fang, L.G.J. de Haart, J. Malzbender, N. Margaritis, et al., Solid Oxide Fuel Cell, Stack and System Development Status at Forschungszentrum Jülich L. Blum, ECS Trans. 68 (2015) 157–169.

[50] L. Blum, L.G.J. de Haart, J. Malzbender, N. Margaritis, N.H. Menzler, Anode-Supported Solid Oxide Fuel Cell Achieves 70 000 Hours of Continuous Operation, Energy Technol. (2016). doi:10.1002/ente.201600114.

[51] V. Petrovsky, M. Gazda, H.U. Anderson, S. Molin, P. Jasinski, Applications of spin coating of polymer precursor and slurry suspensions for Solid Oxide Fuel Cell fabrication, J. Power Sources. 194 (2009) 10–15. doi:10.1016/j.jpowsour.2008.12.054.

[52] S. KOCH, P. Vang Hendriksen, T. JACOBSEN, L. BAY, P. VANGHENDRIKSEN, T. JACOBSEN, et al., Electrical behaviour of strontium-doped lanthanum manganite interfaces, Solid State Ionics. 176 (2005) 861–869. doi:10.1016/j.ssi.2004.11.017.

[53] S. Koch, Contact resistance at ceramic interfaces and its dependence on mechanical load, Solid State Ionics. 168 (2004) 1–11. doi:10.1016/j.ssi.2004.01.010.

[54] X. Sun, M. Chen, Y.-L. Liu, P.V. Hendriksen, M.B. Mogensen, Durability of Solid Oxide Electrolysis Cell and Interconnects for Steam Electrolysis, ECS Trans. 57 (2013) 3229–3238. doi:10.1149/05701.3229ecst.

[55] M. Chen, J.V.T. Høgh, J.U. Nielsen, J.J. Bentzen, S.D. Ebbesen, P.V. V. Hendriksen, High Temperature Co-Electrolysis of Steam and CO 2 in an SOC Stack: Performance and Durability, Fuel Cells. 13 (2013) 638–645. doi:10.1002/fuce.201200169.

[56] S.D. Ebbesen, J. Høgh, K.A. Nielsen, J.U. Nielsen, M. Mogensen, Durable SOC stacks for production of hydrogen and synthesis gas by high temperature electrolysis, Int. J. Hydrogen Energy. 36 (2011) 7363–7373. doi:10.1016/j.ijhydene.2011.03.130.

[57] R.R. Mosbaek, J. Hjelm, R. Barfod, J. Høgh, P. V. Hendriksen, R.R. Mosbæk, Electrochemical Characterization and Degradation Analysis of Large SOFC Stacks by Impedance Spectroscopy, Fuel Cells. 13 (2013) 605–611. doi:10.1002/fuce.201200175.

[58] L. da Conceição, L. Dessemond, E. Djurado, M.M.V.M. Souza, La0.7Sr0.3MnO3-coated SS444 alloy by dip-coating process for metallic interconnect supported Solid Oxide Fuel Cells, J. Power Sources. 241 (2013) 159–167. doi:10.1016/j.jpowsour.2013.04.082.

[59] P. Kodjamanova, Q. Fu, L. Gautier, Electric Current Effects on the Corrosion Behaviour of High Chromium Ferritic Steels, Oxid. Met. (n.d.) 1–12. doi:10.1007/s11085-012-9325-3.

[60] Y. Li, Y. Jiang, J. Wu, R. Pineault, R. Gemmenn, X. Liu, Effect of Electrical Current on Solid Oxide Fuel Cells Metallic Interconnect Oxidation in Syngas, Int. J. Appl. Ceram. Technol. 7 (2010) 41–48. doi:10.1111/j.1744-7402.2009.02430.x.

[61] K. Kawamura, T. Nitobe, H. Kurokawa, M. Ueda, T. Maruyama, Effect of Electric Current on Growth of Oxide Scale on Fe–25Cr Alloy for SOFC Interconnect at 1073 K, J. Electrochem. Soc.

159 (2012) B259. doi:10.1149/2.036203jes.

[62] T. Brylewski, W. Kucza, A. Adamczyk, A. Kruk, M. Stygar, M. Bobruk, et al., Microstructure and electrical properties of Mn1+xCo2−xO4 (0≤x≤1.5) spinels synthesized using EDTA-gel processes, Ceram. Int. 40 (2014) 13873–13882. doi:10.1016/j.ceramint.2014.05.106.

[63] B. Hua, Y. Kong, F. Lu, J. Zhang, J. Pu, J. Li, The electrical property of MnCo2O4 and its application for SUS 430 metallic interconnect, Chinese Sci. Bull. 55 (2010) 3831–3837. doi:10.1007/s11434-010-3161-0.

[64] K.P. Lillerud, P. Kofstad, On High Temperature Oxidation of Chromium, 127 (1979).

[65] S.P. Jiang, X. Chen, Chromium deposition and poisoning of cathodes of solid oxide fuel cells – A review, Int. J. Hydrogen Energy. 39 (2014) 505–531. doi:10.1016/j.ijhydene.2013.10.042.

[66] M.V.F. Schlupp, J.W. Kim, A. Brevet, C. Rado, K. Couturier, U.F. Vogt, et al., Avoiding chromium transport from stainless steel interconnects into contact layers and oxygen electrodes in intermediate temperature solid oxide electrolysis stacks, J. Power Sources. 270 (2014) 587–593. doi:10.1016/j.jpowsour.2014.07.094.

[67] K. Hilpert, Chromium Vapor Species over Solid Oxide Fuel Cell Interconnect Materials and Their Potential for Degradation Processes, J. Electrochem. Soc. 143 (1996) 3642. doi:10.1149/1.1837264.

[68] J.G. Grolig, J. Froitzheim, J.-E. Svensson, Coated stainless steel 441 as interconnect material for solid oxide fuel cells: Oxidation performance and chromium evaporation, J. Power Sources. 248 (2014) 1007–1013. doi:10.1016/j.jpowsour.2013.08.089.

[69] W.N. Liu, X. Sun, E. Stephens, M. Khaleel, Effect of substrate thickness on oxide scale spallation for solid oxide fuel cells, Corros. Sci. 53 (2011) 2406–2412. doi:10.1016/j.corsci.2011.03.025.

[70] X. Sun, W.N. Liu, E. Stephens, M.A. Khaleel, Determination of interfacial adhesion strength

between oxide scale and substrate for metallic SOFC interconnects, J. Power Sources. 176 (2008) 167–174. doi:10.1016/j.jpowsour.2007.10.027.

[71] N.J. Magdefrau, L. Chen, E.Y. Sun, J. Yamanis, M. Aindow, Formation of spinel reaction layers in manganese cobaltite – coated Crofer22 APU for solid oxide fuel cell interconnects, J. Power Sources. 227 (2013) 318–326. doi:10.1016/j.jpowsour.2012.07.091.

[72] W.N. Liu, X. Sun, E. Stephens, M.A. Khaleel, Life prediction of coated and uncoated metallic interconnect for solid oxide fuel cell applications, J. Power Sources. 189 (2009) 1044–1050. doi:10.1016/j.jpowsour.2008.12.143.

[73] D.N. Boccaccini, O. Sevecek, H.L. Frandsen, I. Dlouhy, S. Molin, M. Cannio, et al., Investigation of the bonding strength and bonding mechanisms of SOFCs interconnector–electrode interfaces, Mater. Lett. 162 (2016) 250–253. doi:10.1016/j.matlet.2015.07.137.

[74] J. Froitzheim, G. Meier, L. Niewolak, P. Ennis, H. Hattendorf, L. Singheiser, et al., Development of high strength ferritic steel for interconnect application in SOFCs, J. Power Sources. 178 (2008) 163–173.

[75] S. Molin, M. Chen, P.V. Hendriksen, Oxidation study of coated Crofer 22 APU steel in dry oxygen, J. Power Sources. 251 (2013) 488–495. doi:10.1016/j.jpowsour.2013.09.100.

[76] S.R. Akanda, N.J. Kidner, M.E. Walter, Spinel coatings on metallic interconnects: Effect of reduction heat treatment on performance, Surf. Coatings Technol. 253 (2014) 255–260. doi:10.1016/j.surfcoat.2014.05.049.